



HAL
open science

Understanding the Anomalous J–V Curves in Carbon-Based Perovskite Solar Cells as a Structural Transition Induced by Ion Diffusion

Gilles De Moor, Nicolas Charvin, Cynthia Farha, Toby Meyer, Lara Perrin, Emilie Planes, Lionel Flandin

► **To cite this version:**

Gilles De Moor, Nicolas Charvin, Cynthia Farha, Toby Meyer, Lara Perrin, et al.. Understanding the Anomalous J–V Curves in Carbon-Based Perovskite Solar Cells as a Structural Transition Induced by Ion Diffusion. Solar RRL, 2024, pp.2300998. 10.1002/solr.202300998 . hal-04402188

HAL Id: hal-04402188

<https://hal.science/hal-04402188>

Submitted on 18 Jan 2024

HAL is a multi-disciplinary open access archive for the deposit and dissemination of scientific research documents, whether they are published or not. The documents may come from teaching and research institutions in France or abroad, or from public or private research centers.

L'archive ouverte pluridisciplinaire **HAL**, est destinée au dépôt et à la diffusion de documents scientifiques de niveau recherche, publiés ou non, émanant des établissements d'enseignement et de recherche français ou étrangers, des laboratoires publics ou privés.



Distributed under a Creative Commons Attribution 4.0 International License

Understanding the Anomalous J – V Curves in Carbon-Based Perovskite Solar Cells as a Structural Transition Induced by Ion Diffusion

Gilles De Moor, Nicolas Charvin, Cynthia Farha, Toby Meyer, Lara Perrin, Emilie Planes, and Lionel Flandin*

The investigation of hole transport layer-free mesoporous carbon perovskite solar cells by analyzing current–voltage (J – V) curves under different scan rates, light intensities, and temperatures is presented. A distinctive bump in the curves is identified, previously reported in the literature. The voltage at the inflection point of this transition shows a linear correlation with the scan rate, directly yielding a characteristic relaxation time. Increasing temperature demonstrates a reduction in the magnitude and characteristic time of the bump. It also indicates an activation energy of 0.8 eV, suggesting a diffusion mechanism. Importantly, the intensity of the illumination has no influence on the overall behavior, indicating that the phenomenon is not a photovoltaic processes. It is proposed that the bump originates from transition between a metastable state at high scan rates and a stable one reached after relaxation. To accurately replicate the measured J – V curves, a novel lumped circuit model is introduced and validated. A schematic microstructural model depicts the reversible reduction in photocurrent as a decline in charge transfer capacity caused by the diffusion of large ions at the mesoporous titanium dioxide interface. Ultimately, this study also suggests a plausible reason for the well-known hysteresis commonly observed with perovskite solar cells.

optimize PCE, involving modifications in materials, processing methods, and even the protocols employed for current-voltage (J – V) characterization.^[1] There are very good methods proposed to perform reliable measurements.^[2]

In these intricate systems, the measurement procedure itself can significantly impact PCE measurements. For instance, J – V measurements conducted at high scan rates (SRs) from V_{oc} to 0 V often yield higher PCE values. As a consequence, a majority of “polarization curves” are presented in reverse mode, even though it may not directly relate to practical applications and poses challenges for rationalization.

Irregularities in J – V curves have long been observed across different types of solar cells, manifesting in diverse forms. These irregularities typically indicate a non-optimized system, stemming from the constituent materials or their interactions.^[3]

The disparities between the forward and reverse modes have been extensively discussed in the literature,^[4] particularly in the context of recent perovskite (PK) active layers, where they can exhibit substantial amplitudes. Numerous studies propose various mechanisms to comprehend these differences, often referred to as “hysteresis”. The reversibility of the phenomenon is typically not evaluated through multiple sequential cycles. If the discrepancy arises solely from the first cycle compared to subsequent ones, it could potentially signify a transition between two microstructural states, and this should be stipulated.

The interfaces play a crucial role in these systems due to the incorporation of multiple layers with distinct properties. The thin layers are frequently attributed to the accumulation and release of ionic species, thereby influencing the peculiar macroscopic J – V behavior. The presence of an additional current directly linked to the mobility of charged entities or alterations in the electrical environment within the active layer can further modify the mobility of charge carriers.^[5]

Beyond hysteresis phenomena, other experimental observations indicate the existence of transient phenomena during J – V characterizations. Numerous studies highlight the occurrence of “bumps” on the reverse-mode polarization curves.


1. Introduction

Power conversion efficiency (PCE) serves as a fundamental metric for evaluating the performance of photovoltaic (PV) devices and assessing the quality of new materials and setups. It has become increasingly important to enhance PCE values, sometimes overshadowing the understanding of mechanisms that enable the development of reliable, affordable, and user-friendly cells and materials. Various approaches have been devised to

G. De Moor, N. Charvin, C. Farha, L. Perrin, E. Planes, L. Flandin
Univ. Grenoble Alpes, Univ. Savoie Mont Blanc, CNRS, Grenoble INP,
LEPMI

38000 Grenoble, France
E-mail: lionel.flandin@univ-smb.fr

T. Meyer
Solaronix S.A.
Rue de l'Ouriette 129, 1170 Aubonne, Switzerland

 The ORCID identification number(s) for the author(s) of this article can be found under <https://doi.org/10.1002/solr.202300998>.

DOI: 10.1002/solr.202300998

These bumps are easily recognizable as the current reaches a maximum while reducing the potential from V_{oc} to 0 V. This feature is entirely unexpected, as it would correspond to negative resistance and warrants comprehensive investigation and understanding.

The bump is barely noticeable on planar architectures, but it has already been identified on devices featuring mesoporous interfacial layers and mesoporous insulating layers, such as dye-sensitized solar cells.^[6,7] In these cells, they have been attributed to charge and discharge effects near TiO_2 , which can be influenced by the nature of the cations.

Among the different types of active layers, the presence of bumps in PK solar cells stands out as particularly significant. The characteristics of these bumps, including their shape and size, can vary depending on several factors such as the specific PK material, the manufacturing process, and the device architecture. By optimizing these factors, it is possible to mitigate or even eliminate the occurrence of bumps, thereby enhancing the performance of PK solar cells. However, currently, there is no universal explanation that accounts for the origin of bumps in $J-V$ curves. The phenomenon remains incompletely understood due to the involvement of multiple contributing factors, including trap states, recombination, and transport limitations. Additional research is necessary to gain a comprehensive understanding of the bumps and develop strategies to eliminate them, ultimately improving the performance and stability of PK solar cells.

A decade ago, W. Tress et al. conducted a detailed investigation on bumps observed near the maximum power point (MPP) in $J-V$ curves, which were associated with hysteresis.^[8] They observed that these bumps became more prominent at intermediate SRs but diminished for very slow or fast potential changes. Their findings suggested the presence of a characteristic time associated with this phenomenon. Several other researchers have also studied and provided explanations for these bumps in PK solar cells.

Lee^[9] proposed that incomplete conversion of lead iodide (PbI_2) could lead to the bump shape in $J-V$ curves. Leijtens^[10] associated the bump with ion-induced polarization due to high ion mobility. Jacobsson^[11] attributed a similar observation to surface polarization of the PK active layer at high voltages. Meloni^[12] identified a bump occurring before reaching a current plateau and linked it to the low electric field within the device in reverse mode, affecting the driving force for charge carriers. Nemnes^[13] suggested that the bump originated from cell polarization, which shifted the current response in $J-V$ curves. They developed a polarization model to describe this phenomenon.

Various researchers, such as Ravishankar,^[14] Yan,^[15] and Ren,^[16] have presented different $J-V$ behaviors in solar cells, including a bump where the current near V_{oc} exceeds the short-circuit current. Hwang^[17] attributed the bump to capacitive current resulting from interfacial charge accumulation. Idigoras^[18] proposed recombination at the TiO_2 /PK surface as the main cause of the bump and developed a “drift-diffusion” model. Lopez-Varo^[19] favored the hypothesis of a capacitive charging and discharging mechanism involving ionic accumulation at interfaces. Richardson^[20] identified a significant, yet broad, peak of current in reverse mode and linked it to a delay in charging the Debye layers. Jacobs^[21] and Scognamillo^[22] proposed charge accumulation at the interfaces of the PK layer due

to the presence and migration of mobile ions, along with atomic segregation of halides. Tennyson^[23] observed a bump near the electrical contacts, which they attributed to charge accumulation. Emami^[24] could reduce the bump through optimized thermal treatment, suggesting an imperfection in the active layer microstructure. Sirtl^[25] and Thiesbrummel^[26] observed the bump and associated it with ion drifts in the solar cell.

On the modelling standpoint, many equivalent circuits and structural models have been published. Nemnes^[13] proposed a macroscopic model using an equivalent circuit to describe the dynamic hysteresis and the bump phenomenon. Courtier^[27] developed a “drift-diffusion” model based on the movement of electronic and ionic charges to simulate the bump. Almora^[28] modeled $J-V$ hysteresis using switch-driven currents, providing a good fit to experimental measurements. Anghel^[29] proposed a model resembling a 1-diode model with an additional capacitance, which exhibited an exponential variation of charge with voltage. Alvarez^[30] proposed a model incorporating a delay between changes in system properties and external electric field variations, accounting for photocurrent decay, apparent V_{oc} shift, hysteresis in $J-V$, and a capacitive bump. Boccard^[31] and Li^[32] developed an equivalent circuit related to the microstructure of tandem structures but not specifically designed to describe bumps in $J-V$ curves. In many publications with similar setups, the bump exists but is not further commented.^[33]

In summary, the presence of bumps and dynamic hysteresis in $J-V$ measurements are primarily associated with polarization phenomena resulting from charge accumulation between the PK active layer and its surroundings. These interfacial charges are released during voltage sweeps, resulting in an additional current compared to the normal response. Another factor could be the volume effect within the active layer, altering the electric field and impeding charge diffusion. These two mechanisms are not mutually exclusive.

The main unanswered question is whether the current peak generating the bump corresponds solely to a transient capacitive effect or if it results from a temporary photocurrent. Resolving this question is crucial because the extra capacitive current cannot be utilized to generate energy. In contrast, if the unexpected decrease in current is due to a partial loss of photocurrent, methods could be explored to mitigate the microstructural changes causing this anomaly. The present study aims to provide insights into this critical question and potentially enhance the PCE in the latter case.

2. Experimental Section

2.1. Microstructure

The devices used for this topic were hole transport layer (HTL)-free mesoporous carbon PK (m -CPSM) solar cells and were provided by Solaronix. The architecture of the cell is shown in **Figure 1**. The cell consisted of a glass/FTO front substrate on which an electron-selective layer of compact and mesoporous TiO_2 ($18+/-3$ nm and $550+/-75$ nm respectively) was deposited. A $1+/-0.1$ μm mesoporous ZrO_2 backbone was also added as an insulating layer to avoid Ohmic shorts. Finally, the $17+/-1.5$ μm -thick mesoporous carbon layer was added by

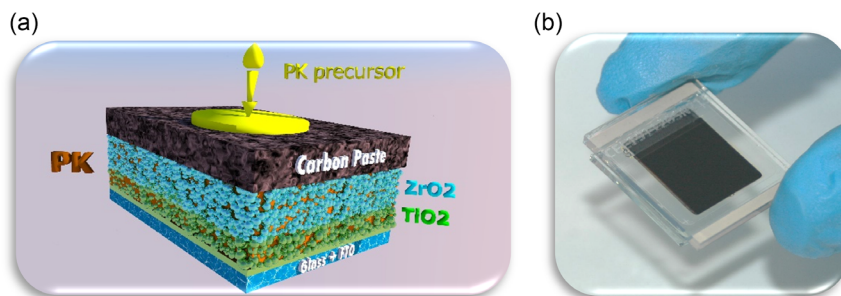


Figure 1. a) Schematic representation of the solar cells and processing method, and b) photograph of the encapsulated cell.

screen printing and acted as HTL. The solution of PK precursor (5-AVA)xMA1-xPbI₃ (part number 76802, Solaronix) in gamma-butyrolactone (GBL) solvent contained lead iodide (PbI₂) and methylammonium iodide (MAI) in equimolar concentration with 5 mol% 5-ammonium valeric acid iodide (5-AVAI). To limit its degradation, the PK was infiltrated at the end of the process by a pipetting method that consisted of a central injection by drop casting. The cells were then encapsulated by hot pressing using a 1.8 mm back glass and a Surlyn gasket. The procedure for the cell preparation is detailed in a very recent reference on the maturation process.^[34]

2.2. Methods

J-V measurements were performed with a Biologic SP-300 potentiostat/galvanostat by illuminating the cells with a Newport Oriel LCS-100 sunlight simulator providing a beam of 1000 W m⁻² light intensity. Prior to *J-V* acquisition, a power calibration was systematically performed using an Oriel solar meter with a calibrated reference silicon cell (Model: 91150 V-Serial number: 801/0871). All measurements on PK devices were performed with a home-made sample holder provided by Solaronix and using a mask with a surface aperture

equal to 0.64 cm². The *J-V* scan was performed in reverse mode from $V_{oc} + 0.1$ V to 0 V. SRs varied from 1 mV s⁻¹, which was close to a steady-state normal use, to fast ones typically 1 V s⁻¹. In order to measure the cell in a reproducible manner, the following steps were used. First, the cell was shorted in the dark before starting the measurement. The open-circuit voltage (OCV) value was then recorded over time, first in the dark for 10 s, and then under light for 150 s to obtain a stable value. The *J-V* characterization was then performed in reverse mode. Finally, another OCV measurement was performed under light for 100 s followed by a 150 s in the dark and then short-circuited during few minutes to return to the equilibrium.

3. Theory and Calculations

3.1. Capacitive Divergence

Figure 2 illustrates the characteristic behavior of current density in reverse mode as a function of voltage for a cell exhibiting an anomaly commonly referred to as a “bump” in the literature.

A comparison is made between our steady-state and dynamic experimental results, obtained with HTL-free carbon-based PK

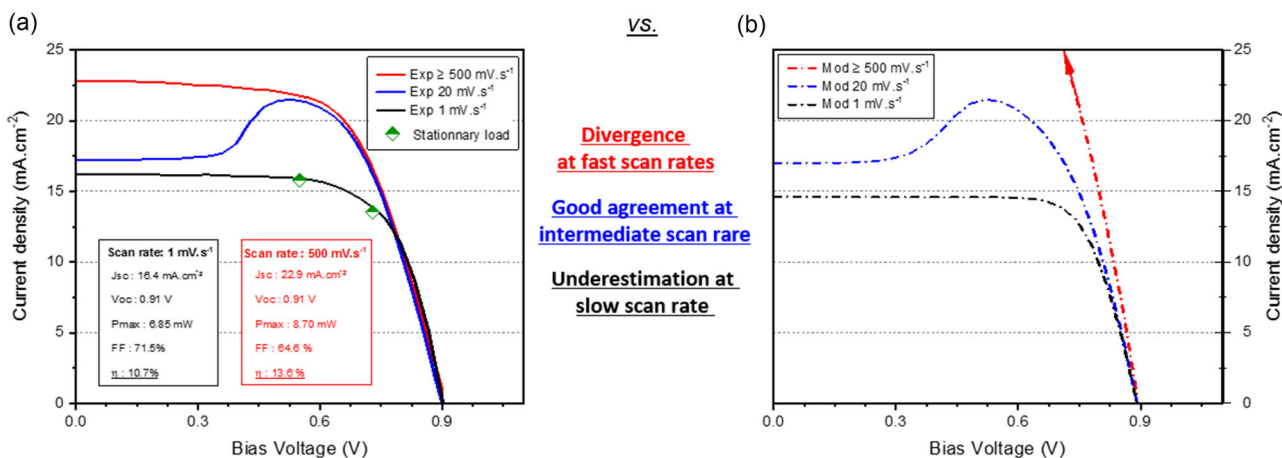


Figure 2. *J-V* curve of a carbon-based PK cell at three different SRs. The experimental results, depicted by the solid lines, exhibit excellent agreement with the simulation based on the equivalent published by Anghel^[29] represented by the dotted lines, particularly for the intermediate SR. However, the simulation predicts a deviation at very high SRs, which contradicts our experimental observations. a) Experimental results. b) Best fit with model described in ref. [29].

solar cells and results calculated from a capacitive model proposed in the literature.^[29] Three different and caricatural SRs are presented to facilitate comparison. Additional measurements were performed by connecting different resistors to the illuminated cell, and the resulting voltage–current data were also plotted on the graph. As expected, all the data points (white/green diamonds) aligned precisely with the stable lower curve. A bump is only observed at intermediate SRs, as previously described.^[8]

Numerical analysis was performed using a lumped model.^[29] This model introduces a modification to the conventional 1D model by including a capacitor that exhibits an exponential relationship with the voltage. This model effectively captures the observed experimental behavior by temporarily increasing the current and generating a characteristic bump in the J – V curve. Figure 2 illustrates the excellent agreement between the published model and the measured experimental data at intermediate SRs. Remarkably, this behavior can be accurately reproduced starting from the 1D model with only a few additional parameters. Table 1 presents the parameter values that best match our experimental results. The authors of that model suggest that the extreme values of the capacitance could potentially stem from the presence of ferroelectric domains, leading to significantly enhanced permittivities. However, this morphological feature has not been corroborated by other analyses, and it fails to explain the exponential dependency of the capacitance on voltage.

In addition, the lumped circuit model with an exponential capacitance deviates from the experimental results in extreme cases. At very low SRs, which are close to real application conditions, the model qualitatively reproduces the typical J – V curve obtained from the 1D model, showing no bumps. However, the model underestimates the quantitative behavior compared to the experiments. In other words, the additional branch in the circuit remains active even after the occurrence of the bump. On the other hand, at very high SRs, the model predicts a linear increase in the capacitive current, following the relationship $i \propto \partial q / \partial t \propto C \times \partial V / \partial t$. However, this contradicts the experimental data shown in Figure 2 at SRs $\geq 500 \text{ mV s}^{-1}$, where the experimental results level off. In this case, the real system appears to reach another state, resembling that of conventional solar cells with an extra 3% gain of efficiency that should be stated in the publications. These quantitative and qualitative discrepancies arising from the “capacitive divergence” using the proposed equivalent models serve as the motivation for the present study and provide an opportunity to develop a new understanding of the J – V curve in PK active layers.

Table 1. Numerical parameters placed in the lumped circuit to best match the experimental data in with the model described by Anghel.^[29]

V_{oc} [V]	R_s [Ω]	I_{ph_stable} [A]	I_{s_stable} [A]	N_{stable}	R_c [Ω]
0.9	25 m	14.5 m	12.5p	1.65	25
R_{s_stable} [Ω]	R_{sh_stable} [Ω]	K	$C0$ [F]	$C1$ [F]	
4.63	11 k	10.5	40 m	85 m	

4. Results and Discussions

4.1. Interrupted Scan Rates

In order to investigate the influence of time on J – V measurements, a time-dependent characterization approach was adopted using constant potentials. The procedure involved three steps and is detailed more specifically in Figure S1, Supporting Information: 1) a fast SR (typically $\geq 500 \text{ mV s}^{-1}$) from V_{oc} to a specified stop bias voltage; 2) a classical chronoamperometry characterization at the stop bias voltage for 60 s; and 3) the J – V curve was completed in the third step, from the stop bias voltage to 0 V at a slow SR of 1 mV s^{-1} .

The experimental results clearly demonstrated that, given sufficient time, all the curves eventually converged to the one obtained at the slow SR, as shown in Figure 3a. This indicates that the any J – V output from the cell lies between the two extreme speeds. They should therefore be viewed as boundaries, we decided to call them the stable and metastable for their characteristics. The lower curve represents the behavior directly relevant to the application in steady conditions, while the upper curve corresponds to the cell sometimes reported in the literature (this artificially improves the PCE).

Based on the previous findings, it is proposed that the upper curve obtained at high SRs represents a metastable state that can only be achieved dynamically. When the SR is halted, the current returns to equilibrium, exhibiting an exponential decay over time (Figure 3b). This exponential decay is characteristic of a relaxation phenomenon and defines a specific time parameter (τ_{inter}). This value is not constant even for a specific cell; it slightly varies depending on the potential at which the measurement is conducted. This results in a narrow distribution of relaxation times, and each individual curve follows a monoexponential decay pattern. While τ_{inter} demonstrates a monotonic variation with the measurement potential (Figure 3a), the extent of variation in this relaxation times remains minimal, within a few seconds.

4.2. A Shifting Bump?

Figure 4a illustrates with a greater precision the influence of SR on reverse J – V characterization (J – V curves in forward mode as a function of SR are shown in Figure S2, Supporting Information). As observed in the previous section, the reverse J – V curves exhibit a typical behavior at both high and low SRs without any bumps. These two experimental J – V -curves were perfectly modeled using a classic 1D model. The parameters and corresponding PCE for the two equivalent circuits are presented in Figure 2a. Despite their significant differences (notably the higher J_{sc} and PCE for the higher SR), both circuits can be considered as conventional PV cells independently. However, this normal behavior at high speed is highly unstable. The presence of a metastable state is confirmed by intermediate SRs, where a gradual decrease in current induces a transition from a state with high current densities to one with lower densities. This transition occurs as a relatively rapid jump within a small voltage range (meaning in a short period of time). The voltage at which this change occurs gradually shifts and appears to be directly influenced by the voltage SR.

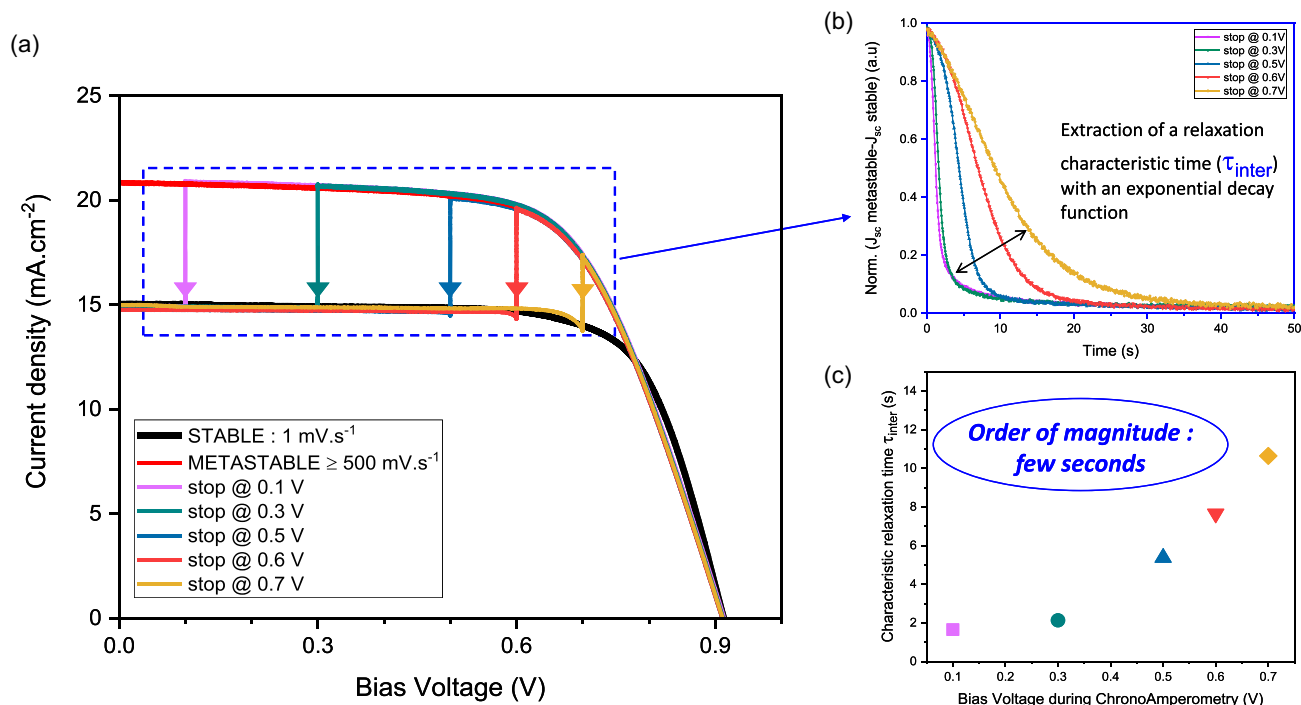


Figure 3. Results obtained from the interrupted SR protocol. a) Evidence for the upper metastable and lower stable boundaries. The transitions between these two states are indicated by arrows in the isopotential chronoamperometry measurements. b) The chronoamperometry results illustrate the exponential relaxation between the metastable state and the stable state. c) Characteristic relaxation time (τ_{inter}) extracted from the chronoamperometry step.

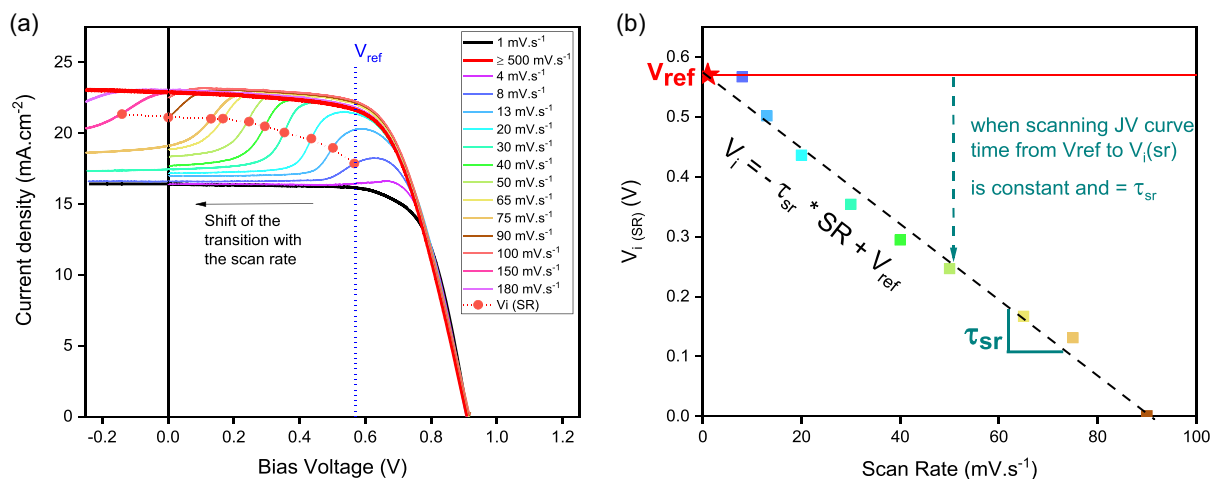


Figure 4. A shifting transition: a) Influence of the SR on the J - V curve in reverse mode. The position of the transition between the metastable and stable states gradually shifts with increasing SR. Red circles indicate the positions of the inflection points (V_i). b) Representation of the V_i as a function of the SR at which they were measured. The resulting dashed line exhibits a constant slope, representing the characteristic time of relaxation (τ_{sr}). In each experiment, the time elapsed between V_{ref} and this line remains constant.

To characterize the transition more precisely, the precise voltage position of the inflection point was determined through derivation and plotted as a function of the SR (Figure 4b and S3, Supporting Information, for more details). Surprisingly, all the obtained points using this simple procedure were found to be well aligned. This measurement was replicated on multiple cells prepared under different conditions and the result with a very reproducible behavior: the voltage at the inflection point

seemed to exhibit a linear dependence on the SR (in contrast to the behavior of the lumped circuit proposed in previous publications).

A straight line characterized by a slope and a y-intercept was thus identified. The slope of this graph represents a time, as the ratio between voltage (V) and SR ($V s^{-1}$). From a numerical standpoint, the slope was found to be ≈ 5 s for this particular cell. This value closely matches the characteristic time obtained

through relaxation methods (τ_{inter}) in Figure 3. Therefore, it is proposed that, mechanistically, these two sets of values essentially correspond to the time required for the conversion from the metastable state (upper curve) to the more stable state (lower boundary). This time will be referred to as the characteristic time determined by the SR (τ_{SR}). The easy determination of this characteristic time enables tracking of the relaxation kinetics. $\tau_{\text{SR}} = 5$ s also implies that the voltage at the inflection point shifts by -5 mV when the SR is increased by 1 mV s^{-1} . The two characteristic times, τ_{inter} and τ_{SR} , clearly represent the same physical mechanism and can be considered equivalent.

The intercept of this line naturally has the physical dimension of voltage and will be referred to as V_{ref} . Based on a relaxation mechanism, V_{ref} corresponds to the voltage at which the relaxation process begins from the upper to the lower curves under equilibrium conditions (SR = 0). In other words, it is the voltage at which the relaxation process initiates, as shown in Figure 4b. The value of V_{ref} holds a different meaning than V_{oc} and has been measured to be smaller for all tested samples (e.g., $V_{\text{ref}} = 0.57$ V, while $V_{\text{oc}} = 0.91$ V). This suggests that prolonged measurement of the current–voltage characteristics at a constant voltage above V_{ref} should not affect the cell or its subsequent relaxation. This straightforward experiment clearly distinguishes the current model, based on relaxation, from previous models assuming an additional capacitive current that increases through a pooling procedure.

To examine the consequences of poling on the J – V curve(s) at different SRs, a cell was subjected to various poling voltages ranging from V_{oc} to “ $V_{\text{oc}} + 0.3$ V” for 3 min (see Figure S4, Supporting Information, for further details). The results are depicted in Figure 5a. Maintaining the cell at a high voltage close to or even above V_{oc} before scanning the J – V curve did not alter the bump. The relaxation mechanism remained largely unchanged. Although the inflection points were slightly shifted toward longer times, the linear behavior persisted, and the characteristic time remained comparable (Figure 5b and Table 2). Thus, the V_{ref} voltage appears to represent a characteristic voltage distinct from V_{oc} .

4.3. Effect of Illumination

J – V measurements were also conducted at different SRs under various illumination intensities, ranging from 0.2 to 1 sun. The results are presented in Figure 6a. As expected, the J_{sc} values are significantly influenced by the solar energy delivered to the cells (see Figure S5, Supporting Information, for further details). However, it is important to note that the increase in J_{sc} with illumination intensity is not linear. This nonlinearity can be attributed to various factors, such as charge recombination losses and temperature elevation due to absorbed light energy. The normalization process revealed a power law behavior with an exponent of 1.38, compatible with the expected result.^[35]

When normalized to the J_{sc} , all cells demonstrate a unique behavior in the graph. Not only the extracted parameters, but the entire curve, including the bump and its correlation with the SR, becomes independent of light intensities. This suggests that the underlying mechanism remains unaffected by the current flowing through the cells. This characteristic is very important for understanding the mechanism and will impact the development of the lumped model.

Plotting the position of the inflection point against the SR provides a quantitative confirmation of the characteristic times. Interestingly, the characteristic times show minimal dependence on the illumination (Figure 6b). Additionally, the reference voltage remains remarkably consistent across various illuminations, despite the cells experiencing different currents. This suggests that the mechanism governing the characteristic time is not directly influenced by the cell’s operational state. The observed transition between the metastable and stable states appears to be a somewhat intrinsic characteristic of the cell.

4.4. Master Curve

It has been demonstrated that the bump observed in the polarization curves corresponds to a transition from a metastable to a more stable state. This transition always occurs in the dynamic regime, after the cell has spent a consistent period of time below

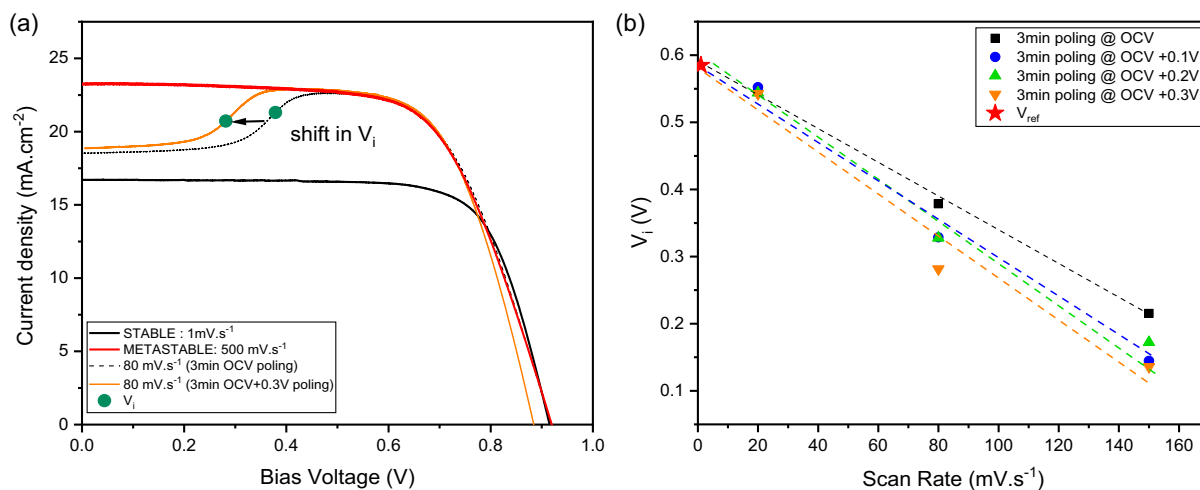


Figure 5. a) Effect of prepoling on the J – V characterization at different voltages around the V_{oc} . b) Determination of the characteristic time by plotting the position of the inflection point versus scan rates. These results are easy to reproduce following a strict experimental protocol.

Table 2. Parameters extracted from J - V curves at different bias poling.

SR [mV s ⁻¹]	OCV poling				OCV + 0.1 V poling			
	OCV [V]	J_{sc} [mA cm ⁻²]	τ_{sr} [s]	V_{ref} [V]	OCV [V]	J_{sc} [mA cm ⁻²]	τ_{sr} [s]	V_{ref} [V]
1	0.92	16.7	2.5	0.59	0.91	16.7	2.8	0.58
20	0.92	17.1			0.90	17.2		
80	0.92	18.5			0.90	18.6		
150	0.92	19.7			0.90	20.0		
300	0.92	23.3			0.89	23.1		
SR [mV s ⁻¹]	OCV + 0.2 V poling				OCV + 0.3 V poling			
	OCV [V]	J_{sc} [mA cm ⁻²]	τ_{sr} [s]	V_{ref} [V]	OCV [V]	J_{sc} [mA cm ⁻²]	τ_{sr} [s]	V_{ref} [V]
1	0.91	16.8	3.1	0.60	0.91	16.8	3.1	0.58
20	0.89	17.1			0.89	17.2		
80	0.89	18.7			0.88	18.9		
150	0.89	20.1			0.88	20.1		
300	0.88	23.2			0.87	23.3		

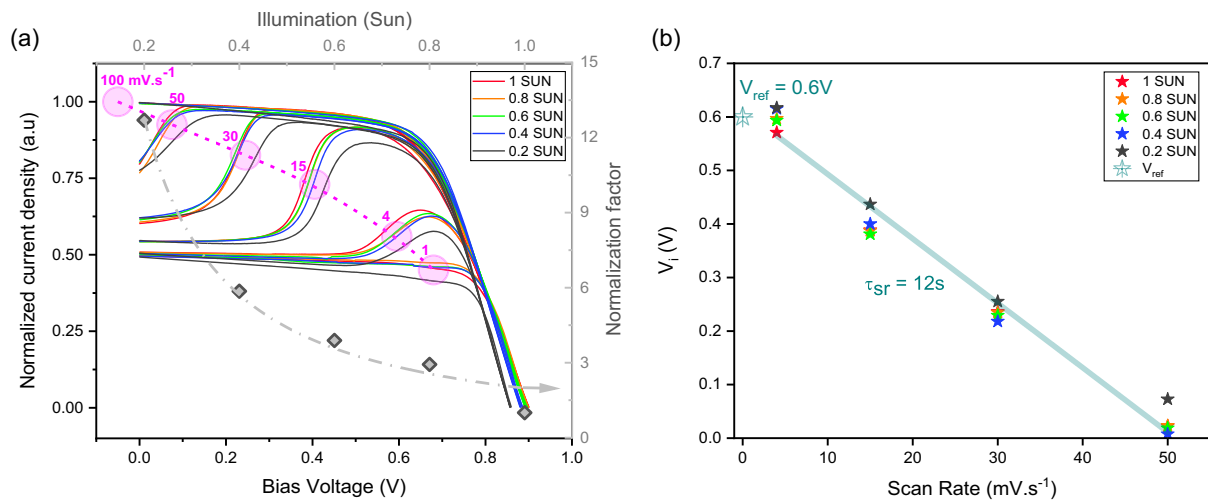


Figure 6. a) The graph illustrates the impact of illumination on J - V characterizations at various SRs, with normalized current density. b) The characteristic relaxation time is determined by plotting the position of the inflection point against the SR. Both extracted parameters, the reference voltage (V_{ref}) at 0.60 ± 0.05 V and the relaxation time (τ_{sr}) at 12.1 ± 0.5 s, were found to be independent of the illumination.

the reference voltage (V_{ref}). The characteristic time (τ_{SR}), ≈ 5 – 10 s, remains close to the relaxation time and is independent of the light intensity. This suggests a close relationship between voltage and time. The similarity in shape obtained for relaxation at different SRs further confirms this relationship.

To convert voltage into time and create a master curve of current density as a function of time, a correction can be applied. The experimental measurement time should be shifted to a master curve time.

$$t_{MC}(V) = t_{exp}(V) - K(SR) \quad (1)$$

with

$$\frac{K(SR)}{t_{MC}(V_{ref})} = 1 \quad (2)$$

By applying this correction, Figure 4a can be replotted as **Figure 7**, with J_{sc} values held constant. Notably, there is a significant disparity in results for negative times, stemming from the differences in time required to reach V_{ref} based on the SR. However, for positive times, once V_{ref} is reached, all the curves converge onto a master curve that is remarkably superimposable. Only runs carried out with very low SRs, which do not exhibit a bump, deviate from this trend. A master curve can be constructed for all other cases without any adjustable parameter, assuming the corrected time is zero at V_{ref} . This provides strong

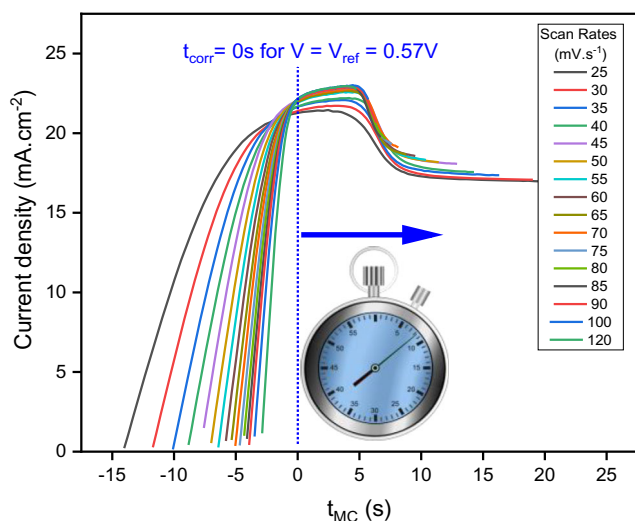


Figure 7. Current density presented as a function of the corrected experimental time (instead of voltage). The time was shifted to take a zero value at V_{ref} as determined in Figure 4b. The plot provides evidence of a master curve in the positive time region, where all the curves converge and exhibit similar behavior.

support for the hypothesis of a transition driven by a diffusion mechanism.

It is noteworthy that the curves with relatively slow SRs do not reach the upper plateau of the J - V curve before their transition. Nevertheless, they follow a similar trend with a slight vertical shift. This indicates that not only is the relaxation time constant for all SRs, but their distribution should also be identical. This will be further explored in the next section.

4.5. Distribution in Relaxation Time

In order to investigate the distribution of the characteristic time in more detail, a probability density function (PDF) is proposed based on the decrease in macroscopic current during the transition. It is hypothesized that the PDF around each most likely characteristic time (defined as the inflection point) is directly proportional to the partial derivative of the current density with respect to time. Essentially, the slope in the J - V curve indicates the relative amount of relaxation, where a steep curve implies a narrow distribution in relaxation time (resulting in a narrow peak in the PDF), and a flatter curve suggests a broader distribution.

With this hypothesis, both the characteristic time and its distribution PDF can be obtained, where

$$PDF(t) \propto \frac{\partial J}{\partial t_{MC}} \quad (3)$$

The $PDF(t)$ curve can be normalized with a suitable parameter λ such that

$$\int_0^{+\infty} \lambda PDF(t) dt = 1 \quad (4)$$

The results of this data treatment are presented in Figure 8.

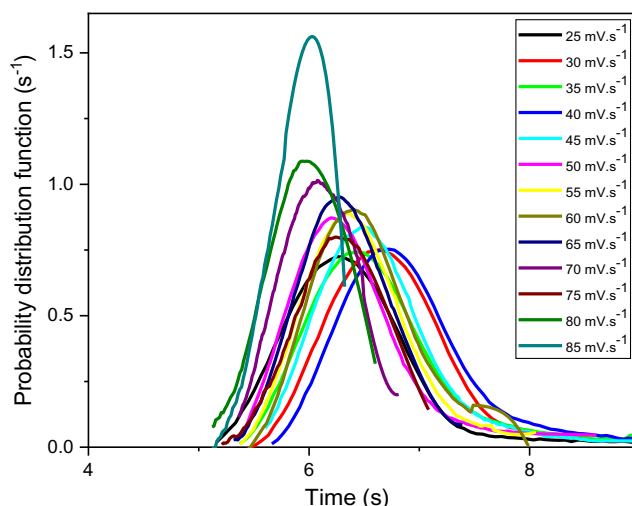


Figure 8. Probability density function (PDF) of the distribution in relaxation time, estimated by the rate at which the cells return to the stable state ($PDF(t) \propto \partial J / \partial t$). This curve is essentially a time derivative of Figure 4a, with the relaxation time defined as zero at V_{ref} . The $PDF(t)$ curve provides insights into the distribution of relaxation times for the cells.

4.6. Effect of Temperature and Activation Energy

Figure 9a demonstrates the temperature dependence of the J - V curve of the PV cell. As the temperature increases,^[36–39] the J - V curve shifts downward and to the right, resulting in a decrease in current output and voltage output. These effects can be attributed to factors such as increased carrier recombination, increased series resistance, reduced bandgap energy, and increased short-circuit current due to thermal energy. Increasing the temperature also affects the amplitude of the bump, with it reducing and nearly disappearing close to 50 °C. The metastable curve is more affected by temperature compared to the stable counterpart. The characteristic time of the transition between the metastable and stable states is reduced, and the amplitude difference between the two states decreases as temperature increases.

Figure 9b illustrates the position of the inflection points as a function of SR at different temperatures. Regardless of the order in which the measurements are carried out, a linear dependence is observed, indicating a well-defined characteristic time. As temperature increases, the characteristic time reduces from a few seconds to a fraction of a second at 50 °C. It is worth noting that the measurement at 50 °C showed a deviation from the gradual evolution observed in the other measurements, possibly due to cell degradation. The inability to construct a single master curve incorporating all J - V characterizations for all temperatures and SRs is attributed to the changes in the amplitude of the bump with temperature.

To align the inflection points for all temperatures, appropriate shift factors are estimated. Using a reference temperature of 30 °C, the SRs are corrected by multiplying them with a constant factor ($a_{SR}(T)$) defined for each temperature as

$$a_{SR}(T) = \frac{V_i(SR, T)}{V_i(SR, T_{ref})} \quad (5)$$

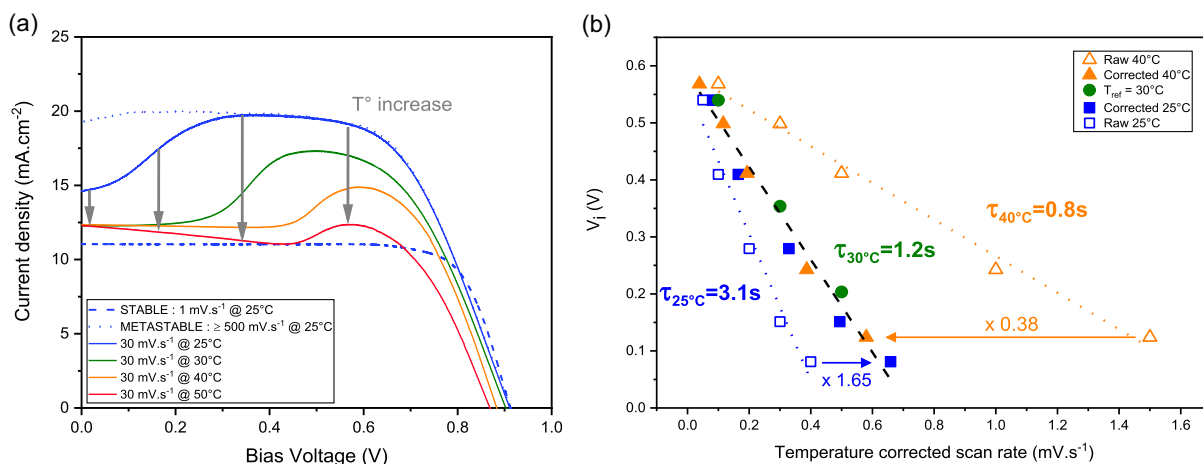


Figure 9. a) Influence of temperature on the J - V characteristic of the cell, measured at a constant SR of 30 mV s^{-1} , which exhibits a well-defined bump. As temperature increases, the J - V curve shifts downward and to the right, indicating a decrease in current and voltage output. b) Relationship between the voltages at the inflection point, determined for various SRs and temperatures. Raw data and shifted SRs according to the Arrhenius law with an activation energy of 0.78 eV (corresponding to 75 kJ mol^{-1}). All data points align along a black dashed line master curve. This method of determining the activation energy differs from the classical method of plotting the logarithm of time versus $1/T$ (temperature). The shift method not only considers the characteristic time for each temperature but also the actual position of each inflection point. The fact that the reference voltage remains constant with temperature indicates its robustness as a parameter, unaffected by whether the cell is operating or by microstructural changes induced by temperature.

On the master curve of inflection voltages as a function of corrected SRs, smooth alignment is achieved for temperatures where the characteristic time can be accurately determined, ranging from 25 to $40 \text{ }^\circ\text{C}$. The best shift factors for $T_{\text{ref}} = 30 \text{ }^\circ\text{C}$ were found to be 0.38 and 1.65 for 40 and $25 \text{ }^\circ\text{C}$, respectively. Figure 9b presents the shift factors (a_T) used for alignment, enabling estimation of the activation energy using the Arrhenius equation. The equation is given by

$$\text{Log} a_{\text{SR}}(T) = -\frac{\alpha E_a}{R} \left(\frac{1}{T} - \frac{1}{T_{\text{ref}}} \right) \quad (6)$$

where α is a constant (0.4347) and R is the ideal gas constant ($8.314 \text{ J mol}^{-1} \text{ K}^{-1}$). The activation energy (E_a) characterizes the minimum energy required for a specific mechanism to occur. In this case, E_a was found to be $\approx 0.78 \text{ eV}$, equivalent to about 75 kJ mol^{-1} . This value is consistent with activation energies reported in the literature for systems with similar temperature-dependent ionic conductivity. The conclusions drawn from this new method align with previous studies,^[40] suggesting that this intermediate value is associated with the diffusion of relatively large ions that have weak interactions with their environment, specifically dipolar interactions.^[41]

4.7. Difference Between Meta- and Stable States

The final data treatment involved subtracting the photocurrents obtained for the stable and metastable states at each voltage value, resulting in a current called J_{diff} . Figure 10 shows the J_{diff} curve, which unexpectedly exhibits a behavior similar to that of a standard photovoltaic device, with three characteristic steps from V_{oc} to 0 V : a linearly increasing region, a knee, and a saturation region. The apparent V_{oc} diff is located between the previously determined V_{ref} and $V_{\text{oc-stab}}$, and there is a progressive slowdown, leading to a slightly sloping line representing an

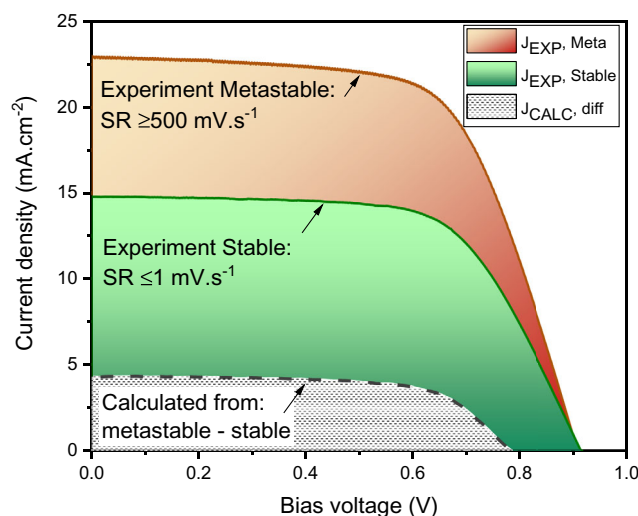


Figure 10. The three distinctive states that can be derived from the cell: stable, metastable and difference show a genuine PV behavior.

apparent short-circuit current (around 5 mA cm^{-2}). The parameters of a 1D model that best fit these experimental data can be determined, as presented in Table 3. Overall, the determination of J - V responses at extreme speeds on the same cell reveals three regular behaviors, each of which can be associated with a simple 1D model. The equivalent circuit values are also provided in Table 3.

4.8. Equivalent Circuit

The 1 diode (1D) lumped circuit is a widely used and classical circuit model to describe the J - V behavior of a solar cell.^[42]

Table 3. Extracted parameters with the 1D equivalent circuit for the three states: 1) metastable, corresponding to the fast scans, 2) stable at low SRs, and 3) diff corresponding to the difference between the two. All three curves are coherent with a classical lumped model for a solar cell.

	V_{oc} [V]	J_{sc} [mA cm^{-2}]	P_m [mW]	V_m [V]	J_m [mA cm^{-2}]	FF [%]
Meta	0.91	22.2	12.9	0.64	19.9	64
Diff	0.78	6.3	3.3	0.59	5.5	66
Stable	0.91	15.8	10.2	0.71	14.2	71

	I_0 [nA]	n	R_s [Ω]	R_{sh} [Ω]
Meta	0.113	1.93	10	1890
Diff	3.4	2.22	17	2794
Stable	0.1	2.00	12	1807

It consists of a single diode and a resistor in parallel, connected in series with a current source representing the photocurrent. The diode represents the nonlinear behavior of the solar cell, while the resistor acts as the internal resistance. By applying Kirchhoff's laws, the voltage and current at any point in the circuit can be determined.^[43–46] The voltage across the diode represents the output voltage of the circuit, while the current through the resistor represents the output current of the circuit, which corresponds to the current generated by the solar cell.

In the present case, the J - V curves revealed three distinct behaviors, including two extreme cases and a third one defined as the difference between the two. The three behaviors resembled the classic behavior of an isolated solar cell and should therefore be viewed as such in the modeling process. Several equivalent circuits were tested to accurately describe the experimental features while minimizing the use of arbitrary parameters, trying to correspond to a physical feature.

The lumped circuit shown in **Figure 11** was found the most suitable. This circuit consists of two independent 1D models representing the stable and difference states. The metastable state was first assumed to be the sum of these two models. To combine the currents from these two models, they were placed in parallel on either side of the voltage output.

To enable the transition between the metastable and stable states, only two additional components were added. Since the characteristic time was crucial in the experiments, the circuit needed to have its own characteristic time (τ_{sw}). The most

reasonable choice was an RC circuit. As the illumination did not affect the transition (**Figure 6a**), the current in this resistance should remain low, regardless of the current produced by the cell. Therefore, a high resistance value (in the $\text{M}\Omega$ range) and a very low capacitance (μF) were used to maintain a characteristic time within the second. A capacitance with a known initial value ($C_{sw} = \frac{\tau_{sw}}{R_{sw}} \approx 1 \mu\text{F}$) was added.

Finally, a switch was incorporated to describe the transition between the two states. The switch was initially closed to allow the diff current to contribute to the overall cell current. It was programmed to open when the charge's capacity shrunk to a specified voltage (V_{sw}). The total cell would then only produce the stable current. The parameter optimization process aimed to match the experimental results by adjusting the parameters of the "switch branch" and reducing the discrepancy between the experimentally obtained position of $V_{i(SR)}$ (**Figure 4a**) and the numerically extracted values using the same technique. No additional parameters were introduced in this process.

A validation of the model was performed using a numerical Simulation Program with Integrated Circuit Emphasis (referred to as SPICE) originally developed at the University of California, Berkeley.^[47] The LTspice version available from Analog Devices was downloaded from their website and utilized, in a very common manner.^[48]

This type of simulation typically requires an initial coherent value for various parameters. A function is then defined to quantify the distance between the experimental results and the modeling. Finally, tools are employed to reduce this distance and optimize the parameter values. However, in the present case, this approach was not feasible due to the strong interaction among different parameters and the high nonlinearity of the system.

Therefore, we started by individually determining the parameter extraction for the two extreme cases, that do not exhibit a bump. The values obtained are indicated in **Table 3**. This leaves us with four parameters to determine: the voltage threshold for opening the switch (V_{sw}), the values of resistance (R_{sw}) and capacitance (C_{sw}) in that branch (both contributing to a characteristic time), and finally, a hysteresis factor proposed in the LTspice tool, which allows for a voltage range to facilitate the switch opening. This last parameter, V_h , ultimately describes the distribution associated with the relaxation observed in **Figure 8**.

To optimize all these parameters and achieve the best possible experimental results, a Python program was written and utilized.

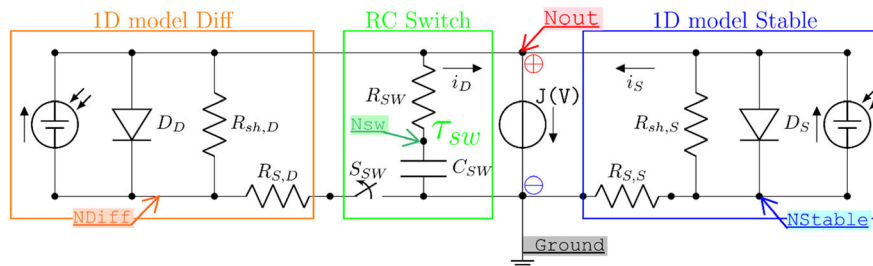


Figure 11. The macroscopic equivalent circuit proposed in this work. It consists of two common 1D models, one of which is temporary (orange) and the other permanent (blue). The switch in the circuit (green) opens in the reverse ramp when the charge on the C_{sw} capacitor decreases below a given value. This switch enables the transition between the metastable state (two photocurrents are added) and the stable state. The estimation of the parameters for this circuit is step wise process, starting with the two 1D models. A minimal working example is presented in SI ("transition.cir" for LTSpice).

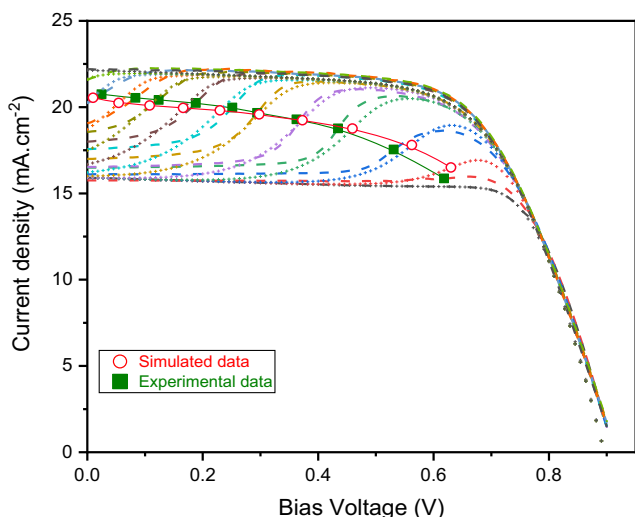


Figure 12. J - V curves obtained from both experimental and modeled data at various SRs (1, 4, 10, 20, 30, 40, 50, 60, 70, 80, 90, 100, 500 mV s^{-1}). The modeled curves were generated using the equivalent circuit depicted in Figure 11 and the values provided in Table 3 for the two 1D models, with specific parameter values assigned to the switch branch ($V_{\text{sw}} = 0.840 \text{ V}$, $R_{\text{sw}} = 3.9 \cdot 10^6 \Omega$, $V_{\text{h}} = -0.45 \text{ V}$, $C_{\text{sw}} = 5.03 \times 10^{-6} \text{ F}$). The upper and lower curves represent genuine characteristic for a solar cell. The upper curve is actually the addition of the two 1D branches. The entire behavior is guided by the switch branch, with a RC circuit and a switch.

By examining the J - V curves at different scanning rates, the model's ability to accurately capture the temporal dependency of the transition is evident. A strong agreement is observed between the experimental data (represented by dashed lines) and the simulated data (represented by crosses), as shown in **Figure 12**. Additionally, open circles and filled squares are included to highlight the inflection voltages (V_i) associated with

characteristic transition times. These markers assist in visually assessing the quality of the fit and further emphasize the fidelity of the model's performance.

Modeling allows confirming the nature of the transition mechanism. It is also verified that the sum of two PV cells also exhibits the behavior of a PV cell. From a microstructural point of view, the two cells are mixed and should be viewed as a single cell in which a very constant fraction of the current is lost during the J - V test. Quantitatively, the modeling reveals a characteristic time different from that of the experiment. Three characteristic times could be identified: 1) in current relaxation at isopotential, 2) through the slope in the $V_i(\text{SR})$ plot, and 3) with the $R_{\text{sw}}C_{\text{sw}}$ product of the equivalent circuit. These three distinct methods roughly lead to the same time, but the simplest and most effective method to estimate it is the slope in the $V_i(\text{SR})$ representation; it is also the most reliable one.

4.9. Simplified Microstructural Model

Figure 13 depicts a simplified microstructural model that aims to explain the presence of a bump in the polarization curve. The model was drawn with a planar interface for the sake of simplicity, but it represents a mechanism compatible with all the experimental observations. The main focus is to highlight that the reversible reduction in short-circuit current density (J_{sc}) is not due to an additional capacitive current, but rather a decrease in either the charge transfer capacity or the photocurrent.

The observed temporal dependencies, particularly the well-defined characteristic time when varying the scanning rate, can be explained by the diffusion time. It is proposed that certain species, possibly relatively large ions, migrate under the influence of an electric field. These species then diffuse within the active layer and accumulate at an interface, impeding the recovery of electrons (or holes) and thereby reducing the macroscopic

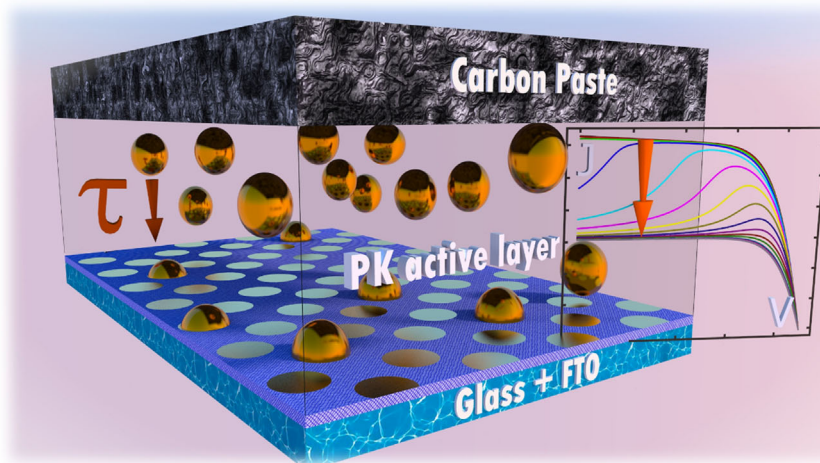


Figure 13. Simplified microstructural model that provides an explanation for the presence of a bump in the J - V curves in reverse mode, without involving capacitive divergence. The model proposes that the ETL-PK interface undergoes a reduction in surface area when it becomes covered by ions. This mechanism leads to a relaxation process with a well-defined characteristic time. The experimental determination of the characteristic time using different methods with consistent results. The bump does not originate from a PV mechanism but changes the J - V curves. The schematic ions presented in this graph could represent different moieties and develop a variety of interfacial problems causing the flux reduction.

current density. Additionally, this accumulation may promote recombination.

The characteristic time obtained for this process aligns with the timescales typically associated with larger charge carriers, such as large ions.^[26] The next challenging step is to carry out more detailed analyses at the interfaces,^[49,50] using impedance measurements during the transient phase between the metastable and stable states, in order to gain a better understanding of the phenomena that lead to that particular photocurrent loss.

5. Conclusion

This experimental study was undertaken with the primary objective of gaining a deeper comprehension of the anomalous behavior detected in certain PK solar cells. Specifically, we investigated instances where a reduction in current manifests during the reverse voltage scanning for PCE determination. This phenomenon is counterintuitively and arguably termed a “bump” in existing literature. This article meticulously describes the methodology used to support the fact that it is actually a structural relaxation between two extreme states.

Given its strong dependence to time, we postulated that varying the SR systematically could serve as a tool to monitor the microstructural changes. Indeed, the gradual shift in voltage location of the inflection points with the SR unambiguously revealed the presence of well-defined characteristic relaxation times.

At extreme SRs, all curves convergence toward two well-defined positions, representing the upper and lower boundaries of the dataset. The lower curve reflected the real operating conditions, while the upper curve represented a transient state lasting ≈ 1 s. This duration, although short for practical use, significantly exceeds the nanosecond-range elementary mechanisms occurring within the solar cell.^[33] In other words, the solar cells effectively operates along the upper curves for an “infinite” time. This vision differs from previous literature that considered the bump as a result of an additional capacitive charge. The observed transition in our cells was distinct from hysteresis behavior and did implied irreversible microstructural evolution.

It was demonstrated that this transition exhibited a characteristic time in the range of seconds, as evidenced by a straight line when plotting the inflection point position against the SR. Moreover, mathematical analysis utilizing partial derivatives of the J - V curve revealed a relatively consistent distribution in relaxation time for a given cell subjected to various scan sweeps.

Two types of master curves were presented: one derived by transforming the scan voltage into a specific equivalent time, and the other based on temperature. Both master curves exhibited high stability in the distribution of relaxation times and indicated the presence of an activation energy of ≈ 70 kJ mol⁻¹.

A macroscopic equivalent circuit was proposed based on the observation that the J - V curve defined with the difference between metastable and stable cells also resembled a solar cell. The metastable cells was defined as the addition of the stable behavior and the new defined difference. The latter was further controlled by a switch defined by analyzing the variation in the intersection point position with the SR. The entire J - V curves

could be reconstructed by independently determining very few parameters, all derived from a direct understanding of the experiments.

The negligible influence of the applied light intensity on the transition itself confirmed that the ultimate mechanism driving this transition was in fact independent of the photovoltaic effect. A lumped equivalent circuit was proposed and verified. It could reproduce the experimental data with very few parameters and lead to the development of a microstructural model explaining the bump phenomenon. The model accounted for SR, temperature dependence, and the effect of elimination. It is also compatible with the value of the activation energy.

In summary, the main objective of this article was to define the “bump” in the J - V curve as a relaxation mechanism, surprisingly independent of the photovoltaic effect. It is therefore theoretically possible to prevent the ion diffusion, thus the interface contamination, and finally to stabilize the photocurrent obtained in the metastable state. By doing that one could use the cells in the upper limit of the J - V curve and thus significantly improve the performances. This has been demonstrated recently with experimental cells.^[51]

Finally we propose, in the meantime, that the solar cells exhibiting similar bumps should be very simply characterized with the parameters from the meta- and stable states, only combined with the easy-to-define characteristic relaxation time and the amplitude of the relaxation (J_{sc_diff}).

Supporting Information

Supporting Information is available from the Wiley Online Library or from the author.

Acknowledgements

This work was funded by both: the European “UNIQUE” project, supported in the SOLAR-ERA.NET_Cofund by ANR, PtJ, MIUR, MINECO-AEI, SWEA (Cofund ERA-NET Action, N° 691664), and the “PROPER” project supported by “EIG Concert Japan” and financed from the French National Centre for Scientific Research under the funding number “IRUEC 222437”. This work was supported by the French National Research Agency, through Investments for Future Program (ref. ANR-18-EURE-0016 – Solar Academy). The Université Savoie Mont Blanc yearly AAP is acknowledged for financial and technical support.

Conflict of Interest

The authors declare no conflict of interest.

Author Contributions

G.D.M. conducted conceptualization, methodology, investigation, formal analysis, and writing. L.F. conducted conceptualization, took care of software, formal analysis, validation, investigation, writing, and supervision. C.F. conducted investigation. N.C. took care of software, formal analysis, methodology, and data curation. L.P. and E.P. took care of investigation and data curation. T.R. took care of resources.

Data Availability Statement

The data that support the findings of this study are available from the corresponding author upon reasonable request.

Keywords

activation energies, characteristic times, hysteresis, ion migrations, perovskites, structural transitions

Received: December 1, 2023

Revised: December 22, 2023

Published online:

- [1] V. M. Le Corre, J. Diekmann, F. Peña-Camargo, J. Thiesbrummel, N. Tokmoldin, E. Gutierrez-Partida, K. P. Peters, L. Perdígón-Toro, M. H. Futscher, F. Lang, J. Warby, H. J. Snaith, D. Neher, M. Stollerfoht, *Sol. RRL* **2022**, *6*, 2100772.
- [2] J. A. Christians, J. S. Manser, P. V. Kamat, *J. Phys. Chem. Lett.* **2015**, *6*, 852.
- [3] K. Mcintosh, *Ph.D. Thesis*, Univ. New South Wales, **2001**.
- [4] G. A. Nemnes, C. Besleaga, V. Stancu, D. E. Dogaru, L. N. Leonat, L. Pintilie, K. Torfason, M. Ilkov, A. Manolescu, I. Pintilie, *J. Phys. Chem. C* **2017**, *121*, 11207.
- [5] R. Gottesman, P. Lopez-Varo, L. Gouda, J. A. Jimenez-Tejada, J. Hu, S. Tirosh, A. Zaban, J. Bisquert, *Chemistry* **2016**, *1*, 776.
- [6] S. Illa, P. Basak, *Sol. Energy* **2018**, *169*, 159.
- [7] H. Elbohy, *Sol. Energy* **2021**, *221*, 375.
- [8] W. Tress, N. Marinova, T. Moehl, S. M. Zakeeruddin, M. K. Nazeeruddin, M. Grätzel, *Energy Environ. Sci.* **2015**, *8*, 995.
- [9] Y. H. Lee, M. Stefiak, L. P. Heiniger, P. Gao, S. Il Seok, M. Grätzel, M. K. Nazeeruddin, in *2014 IEEE 40th Photovolt. Spec. Conf. PVSC 2014*, IEEE, Piscataway, NJ **2014**, 943.
- [10] T. Leijtens, E. T. Hoke, G. Grancini, D. J. Slotcavage, G. E. Eperon, J. M. Ball, M. De Bastiani, A. R. Bowring, N. Martino, K. Wojciechowski, M. D. McGehee, H. J. Snaith, A. Petrozza, *Adv. Energy Mater.* **2015**, *5*, 1.
- [11] T. J. Jacobsson, W. Tress, J. P. Correa-Baena, T. Edvinsson, A. Hagfeldt, *J. Phys. Chem. C* **2016**, *120*, 11382.
- [12] S. Meloni, T. Moehl, W. Tress, M. Franckevičius, M. Saliba, Y. H. Lee, P. Gao, M. K. Nazeeruddin, S. M. Zakeeruddin, U. Rothlisberger, M. Grätzel, *Nat. Commun.* **2016**, *7*, 10334.
- [13] G. A. Nemnes, C. Besleaga, A. G. Tomulescu, I. Pintilie, L. Pintilie, K. Torfason, A. Manolescu, *Sol. Energy Mater. Sol. Cells* **2017**, *159*, 197.
- [14] S. Ravishankar, O. Almora, C. Echeverría-Arroondo, E. Ghahremanirad, C. Aranda, A. Guerrero, F. Fabregat-Santiago, A. Zaban, G. Garcia-Belmonte, J. Bisquert, *J. Phys. Chem. Lett.* **2017**, *8*, 915.
- [15] K. Yan, B. Dong, X. Xiao, S. Chen, B. Chen, X. Gao, H. Hu, W. Wen, J. Zhou, D. Zou, *Sci. Rep.* **2017**, *7*, 6025.
- [16] X. Ren, Z. S. Wang, W. C. H. Choy, *Adv. Opt. Mater.* **2019**, *7*, 1900407.
- [17] T. Hwang, B. Lee, J. Kim, S. Lee, B. Gil, A. J. Yun, B. Park, **2018**, *30*, 1704208.
- [18] J. Idígoras, L. Contreras-Bernal, J. M. Cave, N. E. Courtier, Á. Barranco, A. Borrás, J. R. Sánchez-Valencia, J. A. Anta, A. B. Walker, *Adv. Mater. Interfaces* **2018**, *5*, 1801076.
- [19] P. Lopez-varo, J. A. Jiménez-tejada, M. García-rosell, S. Ravishankar, G. Garcia-belmonte, J. Bisquert, O. Almora, **2018**, 1702772, 1702772.
- [20] G. Richardson, J. M. Foster, *Energy Environ. Sci.* **2019**, *396*, 1702772.
- [21] D. A. Jacobs, Y. Wu, H. Shen, C. Barugkin, F. J. Beck, T. P. White, K. Weber, K. R. Catchpole, *Phys. Chem. Chem. Phys.* **2017**, *19*, 3094.
- [22] A. Scognamiglio, J. Quentin, F. Fu, *Ph.D. Thesis*, Politecnico Di Torino **2019**, <http://webthesis.biblio.polito.it/id/eprint/12614>.
- [23] E. M. Tennyson, B. Roose, J. L. Garrett, C. Gong, J. N. Munday, A. Abate, M. S. Leite, *ACS Nano* **2018**, *13*, 1538.
- [24] S. Emami, J. Martins, D. Ivanou, A. Mendes, *J. Mater. Chem. A* **2020**, *8*, 2654.
- [25] M. T. Sirtl, F. Ebadi, B. T. van Gorkom, P. Ganswindt, R. A. J. Janssen, T. Bein, W. Tress, *Adv. Opt. Mater.* **2021**, *9*, 2100202.
- [26] J. Thiesbrummel, V. M. Le Corre, F. Peña-Camargo, L. Perdígón-Toro, F. Lang, F. Yang, M. Grischek, E. Gutierrez-Partida, J. Warby, M. D. Farrar, S. Mahesh, P. Caprioglio, S. Albrecht, D. Neher, H. J. Snaith, M. Stollerfoht, *Adv. Energy Mater.* **2021**, *11*, 2101447.
- [27] N. E. Courtier, G. Richardson, J. M. Foster, *Appl. Math. Model.* **2018**, *63*, 329.
- [28] O. Almora, P. Lopez-Varo, K. T. Cho, S. Aghazada, W. Meng, Y. Hou, C. Echeverría-Arroondo, I. Zimmermann, G. J. Matt, J. A. Jiménez-Tejada, C. J. Brabec, M. K. Nazeeruddin, G. Garcia-Belmonte, *Sol. Energy Mater. Sol. Cells* **2019**, *195*, 291.
- [29] D. V Anghel, G. A. Nemnes, I. Pintilie, A. Manolescu, *Phys. Scr.* **2019**, *94*, 125809.
- [30] A. O. Alvarez, R. Arcas, C. A. Aranda, L. Bethencourt, E. Mas-Marzá, M. Saliba, F. Fabregat-Santiago, *J. Phys. Chem. Lett.* **2020**, *11*, 8417.
- [31] M. Boccard, C. Ballif, *ACS Energy Lett.* **2020**, *5*, 1077.
- [32] J. Li, H. Wang, X. Y. Chin, H. A. Dewi, K. Vergeer, T. W. Goh, J. W. M. Lim, J. H. Lew, K. P. Loh, C. Soci, T. C. Sum, H. J. Bolink, N. Mathews, S. Mhaisalkar, A. Bruno, *Joule* **2020**, *4*, 1035.
- [33] S. G. Hashmi, D. Martineau, M. I. Dar, T. T. Myllymäki, T. Sarikka, V. Ulla, S. M. Zakeeruddin, M. Grätzel, *J. Mater. Chem. A* **2017**, *5*, 12060.
- [34] E. Planes, C. Farha, G. De Moor, S. Narbey, L. Perrin, L. Flandin, *Sol. RRL* **2023**, *7*, 2300492.
- [35] D. Glowienka, Y. Galagan, *Adv. Mater.* **2022**, *34*, 2105920.
- [36] I. Mesquita, L. Andrade, A. Mendes, *ChemSusChem* **2019**, *12*, 2186.
- [37] M. Jošt, B. Lipovšek, B. Glažar, A. Al-Ashouri, K. Brecl, G. Matič, A. Magomedov, V. Getautis, M. Topič, S. Albrecht, *Adv. Energy Mater.* **2020**, *10*, 2000454.
- [38] J. A. Schwenzer, L. Rakocevic, R. Gehlhaar, T. Abzieher, S. Gharibzadeh, S. Moghadamzadeh, A. Quintilla, B. S. Richards, U. Lemmer, U. W. Paetzold, *ACS Appl. Mater. Interfaces* **2018**, *10*, 16390.
- [39] H. Zhang, X. Qiao, Y. Shen, M. Wang, *J. Energy Chem.* **2015**, *24*, 729.
- [40] M. Leoncini, R. Giannuzzi, A. Giuri, S. Colella, A. Listorti, V. Maiorano, A. Rizzo, G. Gigli, S. Gambino, *J. Sci. Adv. Mater. Devices* **2021**, *6*, 543.
- [41] Y. Inaguma, T. Katsumata, D. Mori, *J. Phys. Soc. Japan* **2010**, *79*, 69.
- [42] A. Ortiz-Conde, F. García-Sánchez, J. Muci, A. Sucre-González, *Facta Univ. - Ser. Electron. Energ.* **2014**, *27*, 57.
- [43] C. Xu, F. Yu, W. Lin, G. Huang, *Crystals* **2018**, *8*, 277.
- [44] A. Khorami, M. Joodaki, *SN Appl. Sci.* **2019**, *1*, 619.
- [45] O. Ourahmoun, *WSEAS Trans. Circuits Syst.* **2020**, *19*, 196.
- [46] S. Lineykin, M. Averbukh, A. Kuperman, *Renew. Sustain. Energy Rev.* **2014**, *30*, 282.
- [47] L. W. Nagel, D. O. Pederson, in *SPICE (Simulation Program With Integrated Circuit Emphasis)*, **1973**.
- [48] K. Sood, N. Ruppert, R. Mahto, *Data Br.* **2022**, *45*, 108581.
- [49] E. Hernández-Balaguera, G. del Pozo, B. Arredondo, B. Romero, C. Pereyra, H. Xie, M. Lira-Cantú, *Sol. RRL* **2021**, *5*, 2000707.
- [50] E. Hernández-Balaguera, L. Muñoz-Díaz, C. Pereyra, M. Lira-Cantú, M. Najafi, Y. Galagan, *Mater. Today Energy* **2022**, *27*, 101031.
- [51] L. Shen, P. Song, L. Zheng, L. Wang, X. Zhang, K. Liu, Y. Liang, W. Tian, Y. Luo, J. Qiu, C. Tian, L. Xie, Z. Wei, *Adv. Mater.* **2023**, *35*, 2301624.